Electrochemical Synthesis of an Organometallic Material Based on Polypyrrole/MnO2 as High-Performance Cathode

Waffa Rakhrour, Djamel Selloum, Abdellah Henni, Noureddine Cherrad, Imene Chikouche, Mokhtar Benalia, Sarra Mouffok, Mabrouk Djedid, Nacira Bouzar, Sophie Tingry

HAL Id: hal-03009668
https://hal.science/hal-03009668

Submitted on 19 Nov 2020

Electrochemical synthesis of an organometallic material based on polypyrrole/MnO$_2$ as high-performance cathode

Waffa Rakhrour[1], Djamel Selloum[1*], Abdellah Henni[1], Noureddine Cherrad[1], Imene Chikouche[2],

Mokhtar Benalia[3], Sarra Mouffok[4], Mabrouk Djedid[3], Nacira Bouzar[3], Sophie Tingry[5]

[1]*Lab. Dynamic Interactions and Reactivity of Systems, Kasdi Merbah University, Ouargla, 30000, Algeria*

[2]*Laboratoire Croissance et Caractérisation de Nouveaux Semi-conducteurs, Université Ferhat Abbas, Sétif-1, Algeria*

[3]*Laboratory of Process Engineering, Laghouat University, Laghouat, Algeria*

[4]*Centre de Recherche Scientifique et Technique en Analyses Physico-Chimiques (CRAPC), Ouargla, 30000, Algeria*

[5]*Institut Européen des Membranes, IEM – UMR 5635, ENSCM, CNRS, Univ Montpellier, Montpellier, France*

* Corresponding Author -mail: selloumdjamel@gmail.com, selloum.djamel@univ-ouargla.dz

(Djamel Selloum)

Abstract

We report herein the design of promising composite material as a cathode in a rechargeable battery by combining the properties of polypyrrole (PPy) and MnO_2 particles. The composites were prepared by electropolymerization of the pyrrole monomer followed by electrodeposition of a manganese salt suspension by two methods. The first method involved the formation of MnO_2 in situ in the PPy/ITO electrode, while the second method involved first a preliminary adsorption of Mn^{2+} ions in the polymer, followed by an electrochemical of the electrode. The morphology of the resulting composite materials (PPy/MnO_2) was studied by Energy-dispersive X-ray spectroscopy (EDS), X-ray diffractometry (XRD), scanning electron microscopy (SEM), Fourier-transform infrared (FTIR). The investigations of the electrochemical properties of the composite electrodes show that the presence of MnO_2 play an important role in improving the surface of polymer films, which leads to lower charge transfer resistance and higher electrode activity. For the optimal synthesis method, the electrode generates a maximum current of up to -7.9 mA.cm^{-2} for the oxygen reduction reaction, which is eight times the current density delivered by the electrode without PPy.

Keywords: composite electrodes; polypyrrol; manganese dioxide; electrodeposition; oxygen reduction

1. Introduction

Energy requirements have led to the intensification of electrochemical generators and batteries [1–4], whose electrochemical performance depends mainly on the nature and structure of the electrode materials (anode and cathode electrodes) [5,6]. The efficiency of these conventional batteries is still limited by a low cyclability [7,8]. Transition metal oxides have been extensively investigated as electrode materials for batteries [9–15]. A great attention has been devoted to manganese dioxide (MnO_2) as cathode material in batteries [16–19] and supercapacitors [20–23], that exhibits high theoretical capacity and can be produced in a cheap and sustainable way [24–31]. However, MnO_2 has a low electronic conductivity that is undesirable in electrochemical devices [32,33], associated with an irreversible reduction in its capacitance at high voltage or high temperature and over several charge-discharge cycles [34–37]. In this regard, considerable research efforts have been devoted to improve the electrochemical performance of MnO_2-based electrodes by combining MnO_2 with highly conductive materials such as metallic nanostructures, carbon nanotubes, graphene or conductive polymers (by polypyrrole, polyaniline, and polythiophene) [38–43]. In a rechargeable battery, the energy storage results from charging the electrical double layer at the electrode and from faradic reactions at the electrolyte interface. To improve the accessibility of electrolytic doping ions to the electrode surface, large-area electro-active electrodes must be constructed, hence the use of conductive polymers to provide a stable conductive environment for the MnO_2 [44–53]. Among them, the conductive properties of polypyrrole (PPy), as well as its low cost, high theoretical specific capacity and good mechanical stability [38,54–57], have been used for the development of high-performance electrodes in supercapacitors, where MnO_2 has been fixed by hydrothermal process [58], by chemical oxidative polymerization in-situ [38,40], or used in the form of nanowires as a matrix [59].

In this work, we choose to insert MnO_2 into PPy films grown by electrochemical polymerization on ITO substrate. We report herein the assessment of two different methods to insert the particles into the polymer matrix. The first method consisted of forming MnO_2 in situ within the PPy/ITO electrode, while the second method involved first a preliminary adsorption of Mn^{2+} ions in the polymer, followed by a subsequent electrochemical reduction step at the electrode. The structural morphology of the resulting composite materials MnO_2/PPy/ITO was carried out by XRD and SEM studies. We performed cyclic voltammetry (CV), LSV (Linear sweep voltammetry) curves and electrochemical impedance spectroscopy (EIS) studies to evaluate oxygen reduction due to the great importance of active cathodes in rechargeable batteries.

2. Experimental

2.1. Chemicals

The monomer pyrrole (99%), $MnCl_2$, KCl, $LiCLO_4$ and acetonitrile were purchased from Sigma-Aldrich.

2.2. Synthesis of PPy and composite film preparation

Electropolymerization of pyrrole monomer was performed onto ITO substrates in a three-electrode cell, with a Pt wire as counter electrode, a saturated calomel electrode (SCE) as the reference electrode and ITO sample (1x2 cm^2) as working electrode, previously cleaned successively with HNO_3, acetone, ethanol and distilled water. The electropolymerization was carried out by cyclic voltammetry over 20 cycles between -1.0 to 1.2 V *vs*. SCE at 20 mV.s^{-1}, in acetonitrile containing 0.1 M of $LiClO_4$ and 0.1 M of Pyrrole [60]. The resulting electrode (estimated area of 1 cm^2), named as PPy/ITO, was thoroughly rinsed with water solution to

remove any remaining monomeric traces. Two different methods have been used to incorporate MnO_2 particles into PPy film.

First method: MnO_2 was electrodeposited directly on a PPy / ITO electrode by performing 10 cycles between 0.4 and 1.5 V (vs SCE) in an aqueous solution of 0.4 M KCl and 0.05 M $MnCl_2$., which we called the "direct method" (d-MnO_2).

Second method: $MnCl_2$ was first adsorbed after simple immersion of a PPy / ITO electrode in an aqueous solution containing 10^{-2} M KCl and 0.05 M $MnCl_2$ for different immersion times (5 and 10 minutes) allowing by electrostatic interactions the exchange of manganese ions with the counterions initially present in the PPy film. A subsequent step of electrochemical reduction resulted in the formation of MnO_2 in the PPy/ITO electrode by cyclic voltammetry (10 cycles) in the potential range of 0.2 - 1.5 V vs SCE in 0.1 M KCl. The second method was called "indirect method" (i-MnO_2).

The resulting composite electrodes were called MnO_2/PPy/ITO.

2.3. Electrode characterization

The XRD were examined by X'Pert Pro MPD X-ray diffractometer using Cu-Kα radiation (λ=0.154059 nm). The FTIR were traced by Nicolet 6700. The electrochemical behavior of the MnO_2/PPy/ITO electrodes with respect to O_2 reduction was evaluated by linear sweep voltammetry (LSV). LSV was conducted from OCP value of 1.4 V to 0 V vs. SCE at a scan rate of 25 mV.s^{-1} in 0.1 M KCl. Electrochemical impedance spectroscopy (EIS) was conducted using Metrohm Autolab (PGSTAT302N) by scanning the frequencies between 100 kHz to 0.1 Hz (10 mV amplitude), at E_{appl} = 0.2 V vs. SCE.

3. Results and discussion

3.1. Characterization of the composite film MnO₂/PPy/ITO

The growth of PPy on ITO is shown on the typical cyclic voltammograms in Fig. 1, characterized by a pair of redox peaks located at 0.5 V *vs.* SCE and attributed to the electrochemical transition from the reduced form of PPy to the oxidized state [28-29]. Inset in Fig. 1 shows the formation of a three-dimensional polymer network observed by SEM characterization.

Fig. 1 Cyclic voltammetry of Pyrrole (0.1 M) at the electrode ITO performed over 20 cycles between -1 and 1.2 V vs. SCE at scanning rate 20 mV.s⁻¹, in the electrolyte 0.1 M LiClO₄ in acetonitrile. Insert: SEM image of PPy/ITO sample.

The MnO₂/PPy/ITO composite films were synthesized by entrapping the metal salt to give metal particles in a subsequent reduction step, using two methods. In the direct method (d-MnO₂), MnO₂ was formed *in situ* on the PPy/ITO electrode from an aqueous solution containing MnCl₂ after ion-exchange subjected to ten successive scans in the potential range starting from the open potential of 0.4 to 1.5 V *vs.* SCE in KCl (Fig. 2a). The CV profile (Fig. 2b) shows the oxidation peak of Mn(+II) in Mn(+IV) located at 1.25 V vs. SCE and the reduction peak of Mn(+IV) in Mn(+II) at 0.65 V vs. SCE, according to the one-step process related to the reaction (1) [61–63].
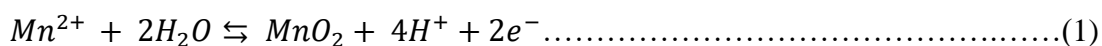
$$Mn^{2+} + 2H_2O \leftrightharpoons MnO_2 + 4H^+ + 2e^- \dots\dots\dots\dots\dots\dots\dots\dots\dots\dots\dots\dots.(1)$$

Fig. 2.(a,b) Cyclic voltammograms of PPy/ITO electrode over 10 scans in the potential range 0.4 - 1.5 V *vs*. SCE in aqueous solution containing 0.4 M KCl and 0.05 M MnCl₂. (c,d) Cyclic voltammograms of ITO/PPy electrode for 10 scans in the potential range 0.2 - 1.5 V vs. SCE in 0.4 M KCl solution, after immersion of the electrode in 10^{-2} M MnCl₂ and 0.4 M KCl solution. Potential scan rate is 20 m V.s⁻¹.

In the indirect method (i-MnO₂), MnO₂ was formed within the PPy/ITO electrode in two successive steps: (i) adsorption of Mn^{2+} ions in the polymer according to two different times of soaking: 5 and 10 minutes, and (ii) formation of metal particles in a subsequent step of electrochemical reduction at the electrode in KCl solution. The resulting cyclic voltammetry, in Fig. 2c, shows an intense peak at 0.9 V corresponding to the oxidation of the incorporated Mn(II) in Mn(IV) on the surface of the PPy/ITO electrode. The lower value of oxidation potential for the second method reflects the easier transformation of Mn^{2+} ions to MnO₂, which are more readily available in the matrix after the absorption step. Furthermore, according to the current density values on the first cyclic voltammetry curves in Figure 2d, a soak time of 5 min for the electrode in the MnCl₂ solution allows the incorporation of increased MnO₂ into the polymer. It can therefore be proposed that MnO₂ acts as electron transfer mediators in the nucleation, formation and growth of the PPy film on the ITO surface.

The morphology of the as-fabricated materials, obtained by cyclic voltammetry, was analyzed by SEM. The nucleation and growth of PPy occurs randomly, forming irregularly shaped particles with defined boundaries, which are typical morphologies of polypyrroles. This morphology depends on the polymerization charge and the nature of the counter anions. Contrary to PPy films characterized by an irregular morphology with remaining particle sizes as nucleation sites varying from 0.10 to 5.0 µm (inset SEM images in Fig.1), the composites electrodes present different morphologies (Fig. 3). For the d-MnO₂ method, the surface morphology of MnO₂/PPy/ITO is characterized (Fig. 3a) by a homogeneous cauliflower-like

structure. For the i-MnO_2 method, the surface morphology of MnO_2/PPy/ITO (Fig. 3a and b) is rather characterized by a smooth and dense layer surrounded by grains. According to the soaking time, the PPy/ITO electrode in Mn^{2+} solution, the grains seem to be localized on the surface of the film for the soaking time of 5 minutes, and rather embedded within the film for the longer soaking time of 10 minutes.

Fig.3 SEM images and EDS of (a,a') d-MnO_2/PPy/ITO, (b,b') i-MnO_2/PPy/ITO(5 min) and (c,c') i-MnO_2/PPy/ITO (10 min).

EDX spectra of the representative electrodes (Fig. 3a',b',c'), qualitatively shows the successful existence of MnO_2 in the PPy matrix with the presence of intense rays at 5.9 and 6.5 keV. The amount of MnO_2 varies with the method of synthesis: with the d-MnO_2 method, it seems that a higher amount is obtained due to the relatively good conductivity of PPy film. In addition, EDX spectra show the presence of carbon, nitrogen, characteristic of the polymer PPy, and the presence of chlorine and oxygen comes from the doping of PPy with perchlorate ions. The presence of Si, In, O and Sn atoms are characteristic of the ITO substrate.

The presence of MnO_2 in the composite electrodes was also confirmed by XRD analyses. Figure 4 presents the pattern of pure PPy, with a broad peak centered at $2\theta = 25°$ assigned to the repeating unit of the pyrrole ring and revealing the amorphous nature of the resulting polymer. This observation is in agreement with PPy materials obtained by classical chemical or electrochemical methods [64,65]. Diffraction peaks indexed by an asterix correspond to the ITO substrate. The two broad peaks at 2θ values of 37.1° and 42.2° correspond to the (131) and (300) crystal planes, respectively, which confirm the crystallographic variety γ-MnO_2 in agreement with the literature (JCPDS no. 14-0644) [66]. Due to the PPy amorphous nature, MnO_2/PPy/ITO samples have an X-ray profile similar to that of pure MnO_2, indicating no noticeable change in crystal structure.

Fig. 4. a: XRD diffraction patterns of MnO₂, PPy/ITO, PPy/MnO₂/ITO (i-MnO₂ and $t_{soaking}$ = 5 min), PPy/MnO₂ (i-MnO₂ and $t_{soaking}$ = 10 min), and PPy/MnO₂/ITO (d-MnO₂). b: FTIR spectra of PPy and PPy/MnO₂ films.

The FTIR spectra of PPy and PPy/MnO₂ films are shown in Figure 4.b. The observed bands confirm the formation of polypyrrole. The absorption bands at 1550, 1450, and 1030 cm^{-1} are characteristic of the C-C, C-N, and C-H stretching vibrations on the PPy rings [67], whereas the bands observed at 1300 and 1160 cm^{-1} correspond to the in-plane deformation of the C-H and the C-N stretching vibrations [68]. The other bands around 1045 cm^{-1} reflect the N-H plane strain vibration of the doped PPy [69]. Although the PPy/MnO₂ and PPy spectra are very similar, we note that the position and the intensity of the characteristic bands of the polypyrrole in PPy/MnO₂ composites are influenced by the insertion of MnO₂, as already observed in the literature [70,71].

3.3. Electrochemical characterization of MnO₂/PPy/ITO

EIS experiments were conducted for further characterizing the PPy/MnO₂/ITO electrodes. Fig. 5 shows the Nyquist plots with are characterized by a typical semicircle in the high frequency region for all samples, which corresponds to the charge transfer resistance (R_{ct}) of the electrodes. For all samples, the semicircle starts at the same value, indicating that the resistance of the electrolyte remains unchanged.

Fig.5. Complex-plane Nyquist impedance plots at E_{appl} = 0.2 V vs. SCE

in 0.1 M KCl, for the electrodes ITO, PPy/ITO, PPy/MnO₂/ITO(i-MnO₂ and tₛₒₐₖᵢₙg = 5

min), PPy/MnO₂(i-MnO₂ and tₛₒₐₖᵢₙg = 10 min), and PPy/MnO₂/ITO (d-MnO₂).

For a given electrode, the lower R_{ct} is, the higher is the electrical conductivity. The results

gathered in Table 1 show that $R_{ct} = 175, 75, 13$ and $8\ \Omega\ cm^2$ for PPy, PPy/d-MnO₂, PPy/i-MnO₂

(5 min) and ITO/PPy i-MnO₂ (10 min), respectively. In the presence of MnO₂, the R_{ct} values

decrease drastically, inducing a lower interfacial charge transfer resistance [72] and thus higher

electrical conductivity of the electrodes compared to PPy. R_{ct} is even lower when MnO₂ was

incorporated in the polymer by the indirect method compared to the direct method. The

modelling of EIS data by a representative equivalent electrical circuit enables the

determination of Q_{CPE} (constant phase element), from the equation $Q_{CPE} = \{(Ci\omega)^{\alpha}\}^{-1}$. The

α values are between 0.66 and 0.83 for all composite electrodes, suggesting the uniformity and

the homogeneity of the materials.

Table 1. Impedance parameters of the composite electrodes.

Given the great importance of the development of electrode materials for O₂ reduction

in batteries, the behavior of the composite electrodes has been studied by LSV from 1.4 to 0 V

vs. SCE in 1M KCl. As shown in Fig.6, the oxygen reduction current starts without

overpotential at 1.4 V vs. SCE, and the current densities show a semi-plateau, resulting from

the control of the electrocatalytic reaction by diffusion of the oxygen to the electrode surface.

The MnO₂/ITO electrode delivers the lowest current density about -0.9 mA.cm⁻², confirming

the crucial role of PPy in improving electrode performance.

Fig. 6. LSV of the composite electrodes ITO/PPy/MnO₂ in aqueous 1 M KCl electrolyte between 1.4 and 0 V vs. SCE at a scan rate of 25 mV s⁻¹.

The maximal current density of O_2 reduction for d-MnO₂/PPy/ITO, i-MnO₂/PPy/ITO(10 min) and i-MnO₂/PPy/ITO(5 min) electrode is -4.9, -7.6 and -7.9 mA.cm⁻², respectively. These values reveal the importance of the synthesis technique used in the design of efficient MnO₂/PPy composites. In the indirect method, we assume that the amount of MnO₂ in PPy affords a close contact between the electrode material and the electrolyte. The maximal current density delivered by i-MnO₂/PPy/ITO(5 min) electrode is -7.9 mA/cm², which is eight times the current density delivered by the electrode without PPy. This result shows the advantage of possible applications of MnO₂ and PPy to prepare efficient electrodes. In comparison with literature, our composite polypyrrole/MnO₂ cathodes have a high and competitive efficiency for oxygen reduction reaction (ORR) with the reported MnO₂ cathodes. As an example, efficient MnO₂-based electrocatalysts have been synthesized for ORR, such as multi-walled MnO₂/PPy/MnO₂ nanotubes [39], or α-MnO₂ nanowires prepared in the presence of an ionic liquid as structure-directing agent [73], able to generate current densities closed to 7 mA.cm⁻². The introduction of nanoparticles into MnO₂ materials has enable ORR to be boosted with delivered current densities close to 6 mA.cm⁻², such as example with Ag in amorphous MnO₂ mixed with carbon nanotubes [74], or with Co_3O_4 attached to the surface of MnO₂ nanorods [75].

4. Conclusion

In this study, MnO₂/PPy electrodes were successfully prepared and examined. The insertion of MnO₂ in the polymer matrix was confirmed by DRX and EDX. SEM micrographs showed cauliflower-like growth on the deposited substrate. MnO₂ grains of similar size were homogeneously distributed in the polymer. The composite electrode showed a decrease in

charge transfer resistance and excellent electrochemical stability. Electrochemical experiments revealed that the composite materials prepared by the direct incorporation of MnO_2 gave the highest performance for O_2 reduction. This study contributes toward advances in the design of efficient MnO_2/PPy composites suitable for rechargeable battery electrodes.

References

1. S. Khamlich, Z. Abdullaeva, J. V. Kennedy, and M. Maaza, Appl. Surf. Sci. **405**, 329 (2017).

2. P. P. Murmu, S. V. Chong, J. Storey, S. Rubanov, and J. Kennedy, Mater. Today Energy **13**, 249 (2019).

3. K. Kaviyarasu, C. Maria Magdalane, D. Jayakumar, Y. Samson, A. K. H. Bashir, M. Maaza, D. Letsholathebe, A. H. Mahmoud, and J. Kennedy, J. King Saud Univ. - Sci. **32**, 1516 (2020).

4. S. S. Rathnakumar, K. Noluthando, A. J. Kulandaiswamy, J. B. B. Rayappan, K. Kasinathan, J. Kennedy, and M. Maaza, Sensors Actuators B Chem. **293**, 100 (2019).

5. J. P. Painuly, Renew. Energy **24**, 73 (2001).

6. K. Bilen, O. Ozyurt, K. Bakırcı, S. Karslı, S. Erdogan, M. Yılmaz, and O. Comaklı, Renew. Sustain. Energy Rev. **12**, 1529 (2008).

7. B. Dunn, H. Kamath, and J.-M. Tarascon, Science **334**, 928 (2011).

8. J. Chow, R. J. Kopp, and P. R. Portney, Science (80-.). **302**, 1528 LP (2003).

9. B.-O. Park, C. D. Lokhande, H.-S. Park, K.-D. Jung, and O.-S. Joo, J. Power Sources **134**, 148 (2004).

10. H.-K. Kim, T.-Y. Seong, J.-H. Lim, W. Ii Cho, and Y. Soo Yoon, J. Power Sources **102**, 167 (2001).

11. C.-C. Hu and K.-H. Chang, J. Power Sources **112**, 401 (2002).

12. A. K. Noordeen, S. Sambasivam, S. Chinnasamy, J. Ramasamy, and T. Subramani, J. Inorg. Organomet. Polym. Mater. **28**, 73 (2018).

13. M. Yeganeh Shad, M. Nouri, A. Salmasifar, H. Sameie, R. Salimi, H. Eivaz Mohammadloo, A. A. Sabbagh Alvani, M. Ashuri, and M. Tahriri, J. Inorg. Organomet. Polym. Mater. **23**, 1226 (2013).

14. M. M. Doeff, J. Cabana, and M. Shirpour, J. Inorg. Organomet. Polym. Mater. **24**, 5 (2014).

15. S. E. H. Etaiw and M. S. Ibrahim, J. Inorg. Organomet. Polym. Mater. **23**, 340 (2013).

16. M. Toupin, T. Brousse, and D. Bélanger, Chem. Mater. **16**, 3184 (2004).

17. R. N. Reddy and R. G. Reddy, J. Power Sources **132**, 315 (2004).

18. C.-C. Hu and T.-W. Tsou, J. Power Sources **115**, 179 (2003).

19. R. N. Reddy and R. G. Reddy, J. Power Sources **124**, 330 (2003).

20. J. Zhou, H. Zhao, X. Mu, J. Chen, P. Zhang, Y. Wang, Y. He, Z. Zhang, X. Pan, and E. Xie, Nanoscale **7,** 14697 (2015).

21. R. Rostami and M. Faraji, J. Inorg. Organomet. Polym. Mater. (2020).

22. S. K. Kandasamy and K. Kandasamy, J. Inorg. Organomet. Polym. Mater. **28**, 559 (2018).

23. J. Zhang, J. Chen, Q. Zhang, R. Wang, and S. Wu, J. Inorg. Organomet. Polym. Mater. **29**, 1400 (2019).

24. F. Liao, X. Han, D. Cheng, Y. Zhang, X. Han, C. Xu, and H. Chen, Ceram. Int. **45**, 1058 (2019).

25. Q. Wang, Y. Ma, X. Liang, D. Zhang, and M. Miao, Chem. Eng. J. **371**, 145 (2019).

26. Y. Chai, Z. Li, J. Wang, Z. Mo, and S. Yang, J. Alloys Compd. **775**, 1206 (2019).

27. W. Guo, C. Yu, S. Li, Z. Wang, J. Yu, H. Huang, and J. Qiu, Nano Energy **57**, 459 (2019).

28. P. Zhao, M. Yao, H. Ren, N. Wang, and S. Komarneni, Appl. Surf. Sci. **463**, 931 (2019).

29. M. S. Kolathodi, M. Palei, T. S. Natarajan, and G. Singh, Nanotechnology **31**, 125401 (2020).

30. S. Hong, X. Huang, H. Liu, and Z. Gao, J. Inorg. Organomet. Polym. Mater. **29**, 1587 (2019).

31. S. Wu, J. Zhang, C. Sun, and J. Chen, J. Inorg. Organomet. Polym. Mater. (2020).

32. P. Lv, Y. Y. Feng, Y. Li, and W. Feng, J. Power Sources **220**, 160 (2012).

33. S. Grover, S. Shekhar, R. K. Sharma, and G. Singh, Electrochim. Acta **116**, 137 (2014).

34. J.-W. Wang, Y. Chen, and B.-Z. Chen, J. Electrochem. Soc. **162**, A1654 (2015).

35. S. R. Sivakkumar, J. M. Ko, D. Y. Kim, B. C. Kim, and G. G. Wallace, Electrochim. Acta **52**, 7377 (2007).

36. H. Xia, M. O. Lai, and L. Lu, JOM J. Miner. Met. Mater. Soc. **63**, 54 (2011).

37. K.-T. Lee, C.-B. Tsai, W.-H. Ho, and N.-L. Wu, Electrochem. Commun. **12**, 886 (2010).

38. S. A. El-Khodary, I. S. Yahia, H. Y. Zahran, and M. Ibrahim, Phys. B Condens. Matter **556**, 66 (2019).

39. H. Yuan, L. Deng, J. Tang, S. Zhou, Y. Chen, and Y. Yuan, ChemElectroChem **2**, 1152 (2015).

40. R. Mahore, D. Burghate, S. Kondawar, A. Mahajan, and D. Nandanwar, Adv. Mater. Lett. **9**, 538 (2018).

41. G. Yu, L. Hu, M. Vosgueritchian, H. Wang, X. Xie, J. R. McDonough, X. Cui, Y. Cui, and Z. Bao, Nano Lett. **11**, 2905 (2011).

42. J. Chen, Y. Wang, J. Cao, Y. Liu, J.-H. Ouyang, D. Jia, and Y. Zhou, Electrochim. Acta **182**, 861 (2015).

43. J. Bo, X. Luo, H. Huang, L. Li, W. Lai, and X. Yu, J. Power Sources **407**, 105 (2018).

44. A. Bahloul, B. Nessark, N. Chelali, H. Groult, A. Mauger, and C. M. Julien, Solid State Ionics **204**–**205**, 53 (2011).

45. H. Zouaoui, D. Abdi, A. Bahloul, B. Nessark, E. Briot, H. Groult, A. Mauger, and C. M. Julien, Mater. Sci. Eng. B 1 (2016).

46. W. Ni, D. Wang, Z. Huang, J. Zhao, and G. Cui, Mater. Chem. Phys. **124**, 1151 (2010).

47. M. Nakayama, Y. Kashiwa, and K. Suzuki, J. Electrochem. Soc. **156**, D125 (2009).

48. Q. Lu and Y. Zhou, J. Power Sources **196**, 4088 (2011).

49. E. C. Rios, A. V Rosario, R. M. Q. Mello, and L. Micaroni, J. Power Sources **163**, 1137

(2007).

50. S. Karastogianni and S. Girousi, Anal. Chem. Insights **2016**, 1 (2016).

51. H. Khan, K. Malook, and M. Shah, J. Mater. Sci. Mater. Electron. **29**, 9090 (2018).

52. M. Wang, Q. Yang, T. Zhang, B. Zhu, and G. Li, RSC Adv. **6**, 19952 (2016).

53. N. Boudissa, F. Z. Satour, A. Zouaoui, H. Benamrani, and A. Zegadi, J. Inorg.

Organomet. Polym. Mater. **30**, 2677 (2020).

54. R. P. Mahore, D. K. Burghate, S. B. Kondawar, A. P. Mahajan, and D. V. Nandanwar,

Adv. Mater. Lett. **9**, 538 (2018).

55. S. Shivakumara and N. Munichandraiah, J. Alloys Compd. **787**, 1044 (2019).

56. A. Bahloul, B. Nessark, E. Briot, H. Groult, A. Mauger, K. Zaghib, and C. M. Julien, J.

Power Sources **240**, 267 (2013).

57. J. Ji, X. Zhang, Z. Huang, X. Yu, H. Huang, Y. Huang, and L. Li, J. Nanosci.

Nanotechnol. **17**, 4356 (2017).

58. P. Li, Y. Yang, E. Shi, Q. Shen, Y. Shang, S. Wu, J. Wei, K. Wang, H. Zhu, and Q. Yuan,

ACS Appl. Mater. Interfaces **6**, 5228 (2014).

59. J. Zhang, Y. Shi, Y. Ding, W. Zhang, and G. Yu, Nano Lett. **16**, 7276 (2016).

60. J. H. Kaufman, J. Electrochem. Soc. **131**, 2092 (1984).

61. R. Inoue and M. Nakayama, ECS Trans. **41**, 83 (2012).

62. S. Nijjer, J. Thonstad, and G. M. Haarberg, Electrochim. Acta **46**, 395 (2000).

63. J.-P. Petitpierre, C. Comninellis, and E. Plattner, Electrochim. Acta **35**, 281 (1990).

64. X. Chen, L. Liu, Z. Yan, Z. Huang, Q. Zhou, G. Guo, and X. Wang, RSC Adv. **6**, 2345

(2016).

65. J.-G. Wang, B. Wei, and F. Kang, Rsc Adv. **4**, 199 (2014).

66. W. Si, Y. Wang, Y. Peng, X. Li, K. Li, and J. Li, Chem. Commun. **51**, 14977 (2015).

67. L. Yuan, C. Wan, and L. Zhao, Int. J. Electrochem. Sci. **10**, 9456 (2015).

68. J. Jang and J. H. Oh, Adv. Funct. Mater. **15**, 494 (2005).

69. Y. C. Jung, N. G. Sahoo, and J. W. Cho, Macromol. Rapid Commun. **27**, 126 (2006).

70. C. Wang, W. Wan, J.-T. Chen, H.-H. Zhou, X.-X. Zhang, L.-X. Yuan, and Y.-H. Huang, J. Mater. Chem. A **1**, 1716 (2013).

71. X. Liang, M. Zhang, M. R. Kaiser, X. Gao, K. Konstantinov, R. Tandiono, Z. Wang, H.-K. Liu, S.-X. Dou, and J. Wang, Nano Energy **11**, 587 (2015).

72. X. Fan, X. Wang, G. Li, A. Yu, and Z. Chen, J. Power Sources **326**, 357 (2016).

73. Y. Gu, G. Yan, Y. Lian, P. Qi, Q. Mu, C. Zhang, Z. Deng, and Y. Peng, Energy Storage Mater. **23**, 252 (2019).

74. H. Sun, Z. Hu, J. Yu, and Z. Du, J. Electrochem. Soc. **167**, 080539 (2020).

75. C. Cui, G. Du, K. Zhang, T. An, B. Li, X. Liu, and Z. Liu, J. Alloys Compd. **814**, 152239 (2020).

Table 1. Impedance parameters of the composite electrodes.

Sample	Z_{CPE} (μF /cm^2)	R_{ct}(kΩ cm^2)	α
ITO	137.9	222.6	0.83
ITO/PPy	138.7	174.7	0.78
ITO/PPy/d-MnO$_2$	153.4	75.0	0.66
ITO/PPy/i-MnO$_2$(5 min)	178.6	13.1	0.67
ITO/PPy i-MnO$_2$(10 min)	194.1	8.2	0.74
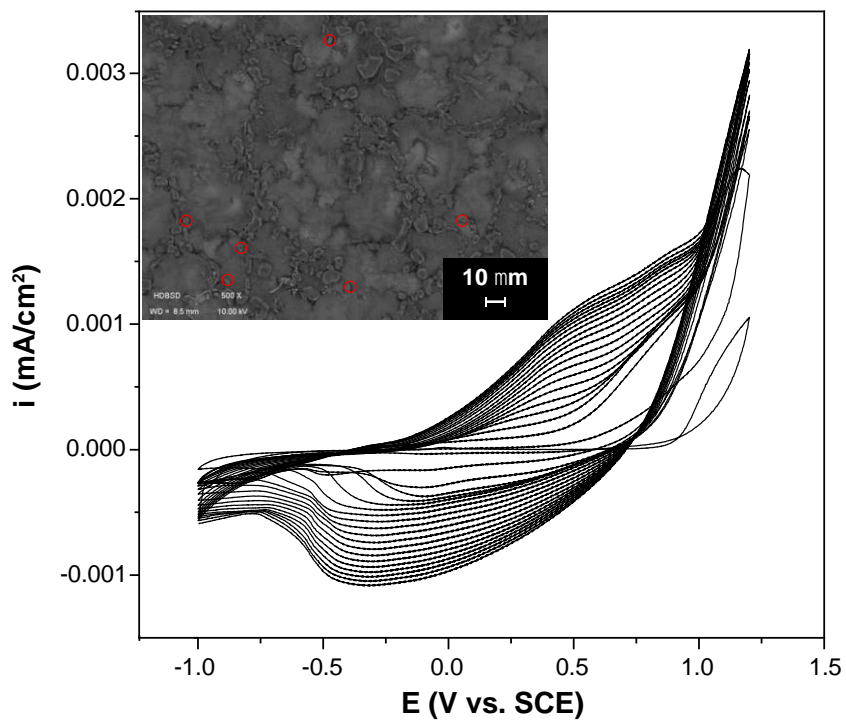
Fig. 1 Cyclic voltammetry of Pyrrole (0.1 M) at the electrode ITO performed over 20 cycles between -1 and 1.2 V vs. SCE at scanning rate 20 mV.s^{-1}, in the electrolyte 0.1 M LiClO$_4$ inacetonitrile. Insert: SEM image of PPy/ITO sample
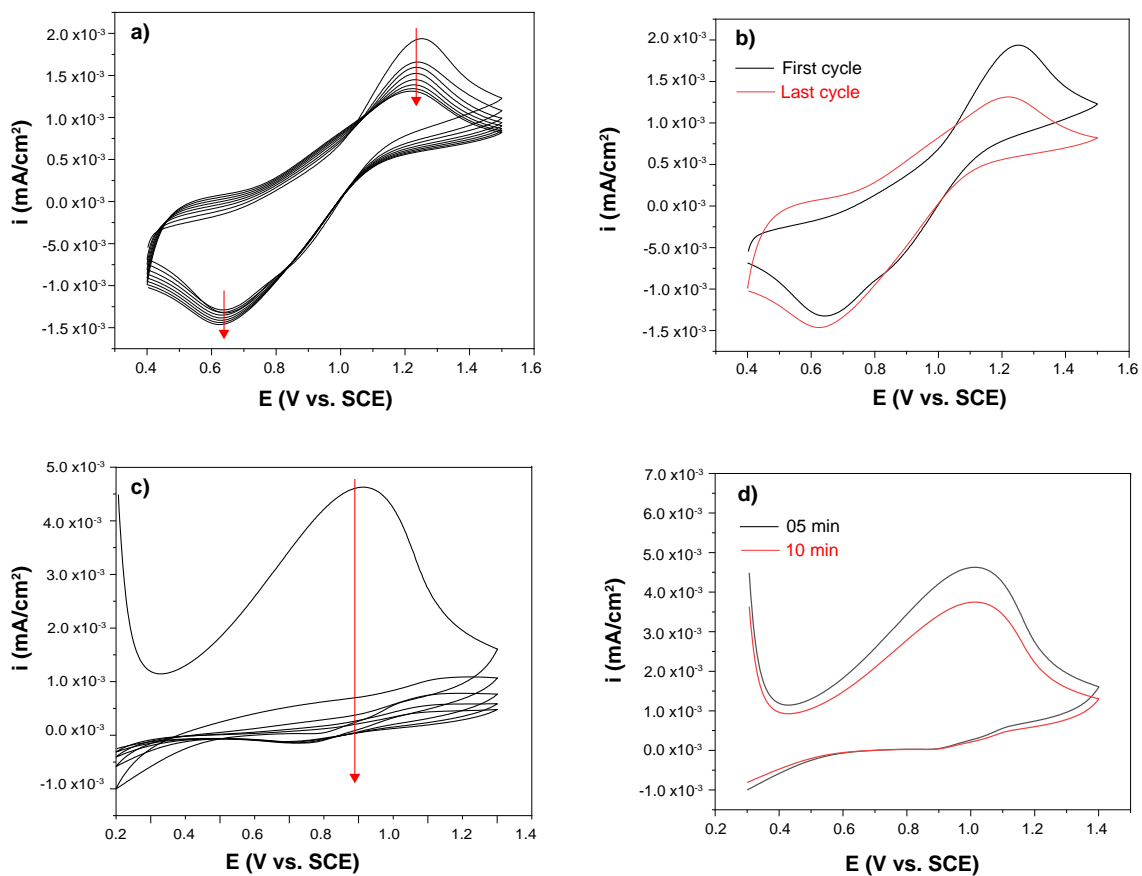
Fig. 2. (a,b) Cyclic voltammograms of PPy/ITO electrode over 10 scans in the potential range 0.4 - 1.5 V *vs.* SCE in aqueous solution containing 0.4 M KCl and 0.05 M $MnCl_2$. (c,d) Cyclic voltammograms of ITO/PPy electrode for 10 scans in the potential range 0.2 - 1.5 V vs. SCE in 0.4 M KCl solution, after immersion of the electrode in 10^{-2} M $MnCl_2$ and 0.4 M KCl solution. Potential scan rate is 20 m $V.s^{-1}$.
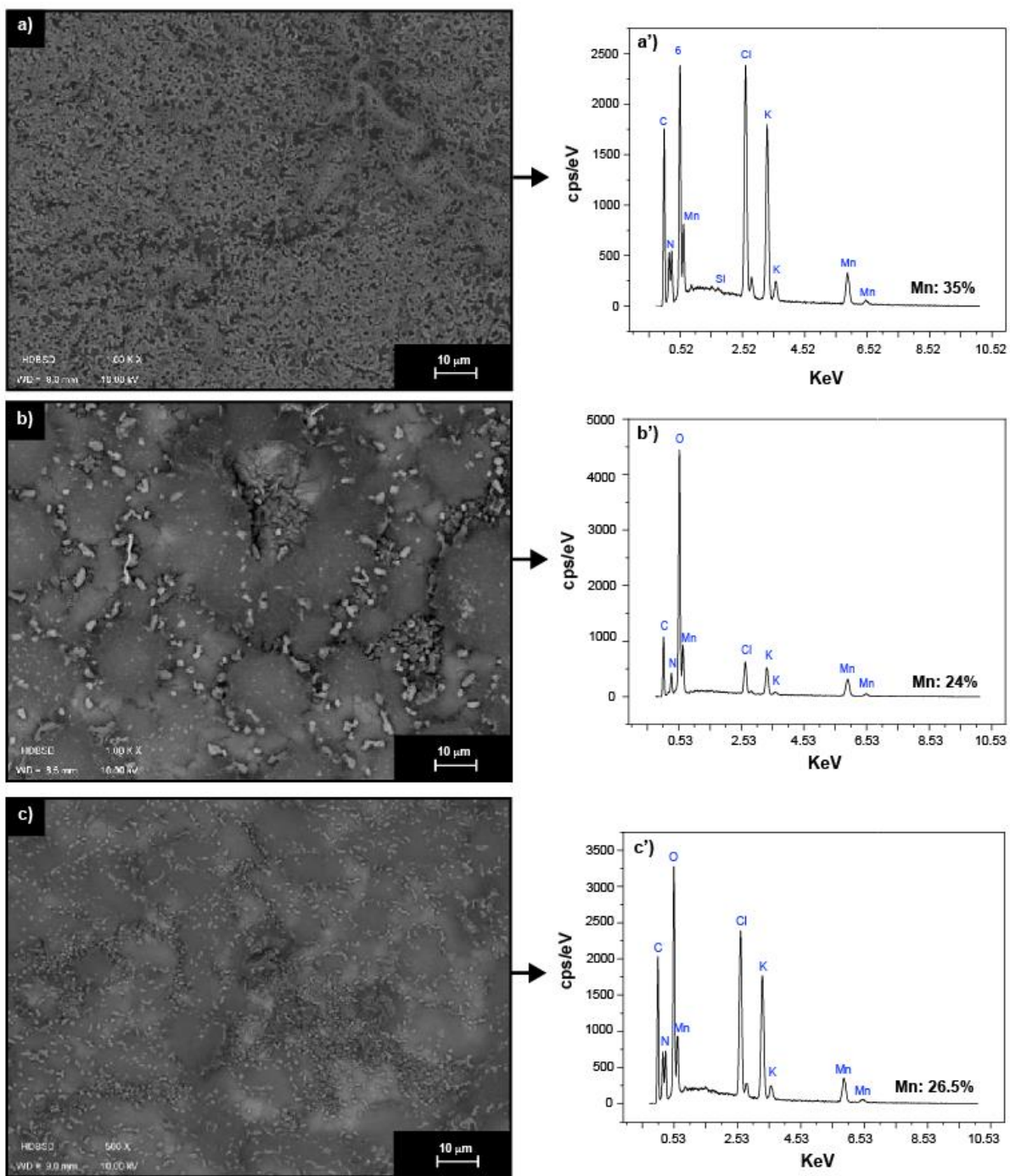
Fig.3 SEM images and EDS of (a,a') d-MnO_2/PPy/ITO, (b,b') i-MnO_2/PPy/ITO(5 min) and (c,c') i-MnO_2/PPy/ITO (10 min).
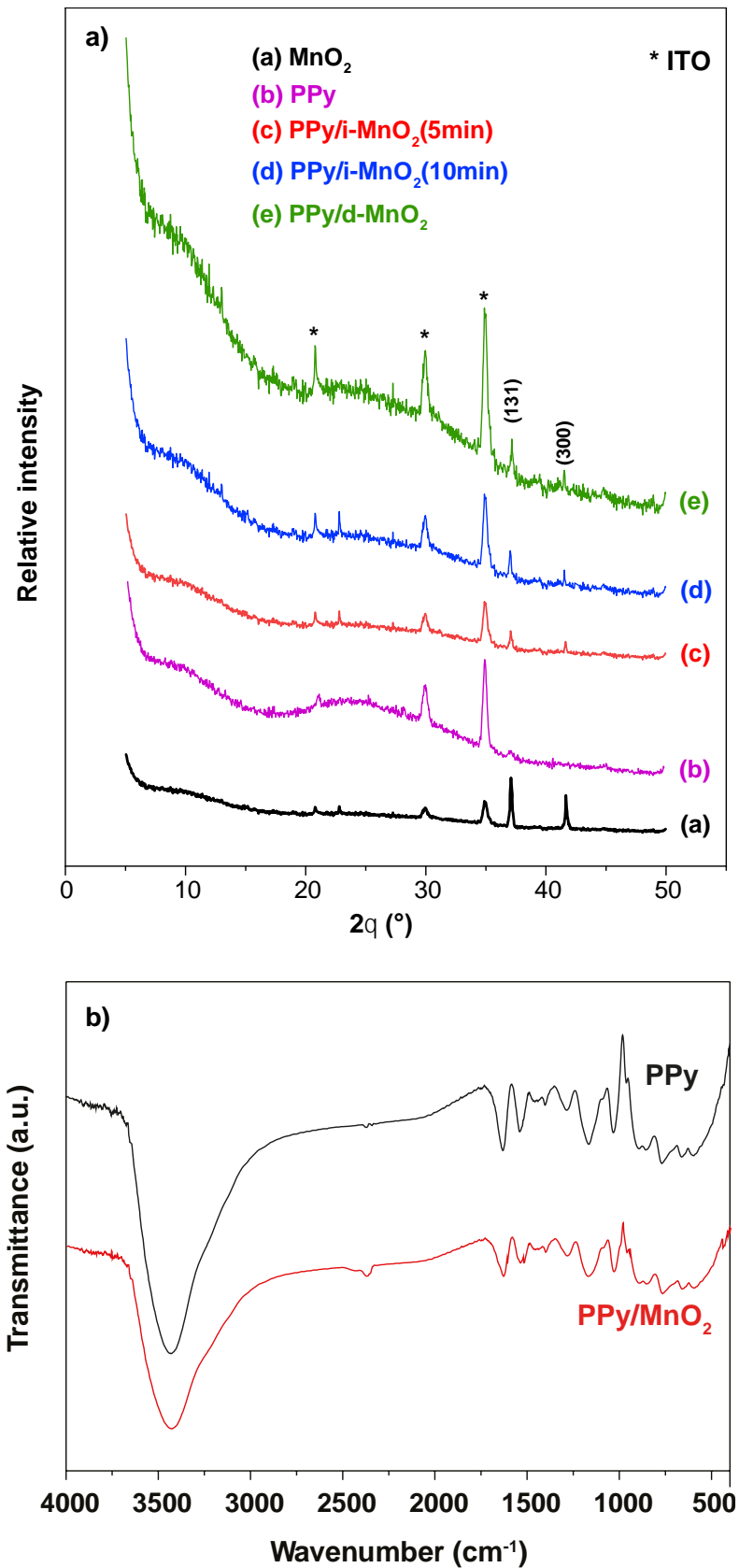
Fig. 4. a: XRD diffraction patterns of MnO_2, PPy/ITO, PPy/MnO_2/ITO (i-MnO_2 and $t_{soaking}$ = 5 min), PPy/MnO_2 (i-MnO_2 and $t_{soaking}$ = 10 min), and PPy/MnO_2/ITO (d-MnO_2). b: FTIR spectra of PPy and PPy/MnO_2 films.
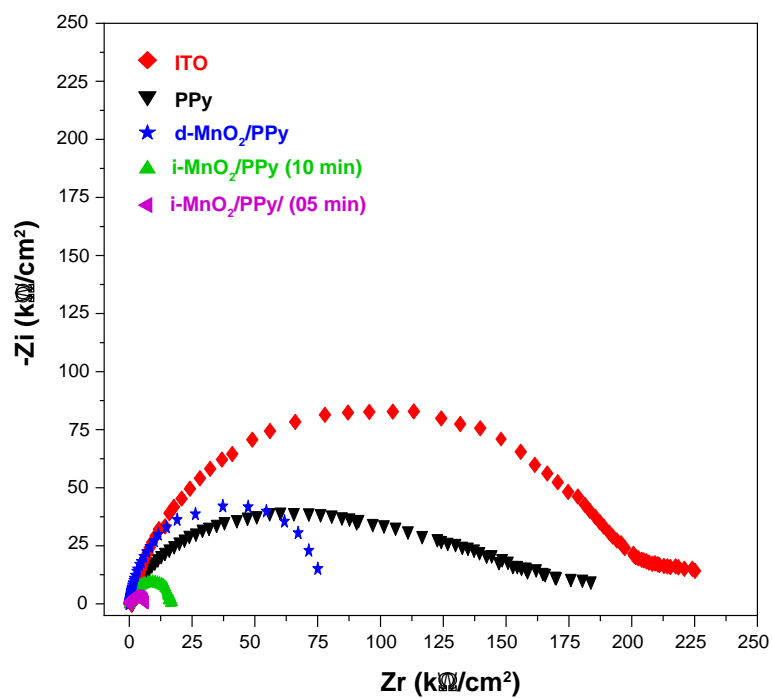
Fig.5. Complex-plane Nyquist impedance plots at $E_{appl} = 0.2$ V vs. SCE

in 0.1 M KCl, for the electrodes ITO, PPy/ITO, PPy/MnO$_2$/ITO(i-MnO$_2$ and t$_{soaking}$ = 5 min),

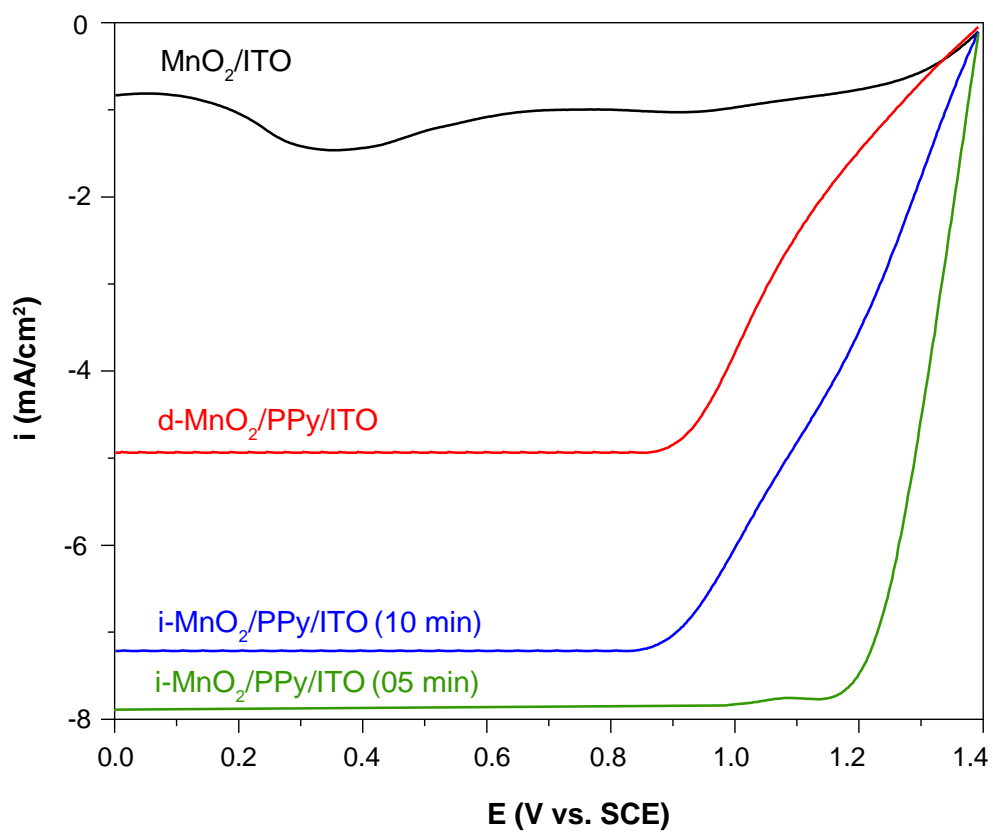PPy/MnO$_2$(i-MnO$_2$ and t$_{soaking}$ = 10 min), and PPy/MnO$_2$/ITO (d-MnO$_2$).

Fig. 6. LSV of the composite electrodes ITO/PPy/MnO$_2$ in aqueous 1 M KCl electrolyte

between 1.4 and 0 V vs. SCE at a scan rate of 25 mV.s^{-1}.